# Journal of Materials Chemistry C

## COMMUNICATION

Check for updates

# A tuneable ionic memristor based on bipolar electrochemistry

Kin Wa Kwan [ID] * and Alfonso Hing Wan Ngan*

The advancement of neuromorphic computing is driven by progress in computing hardware and architecture. For further improving the energy efficiency of computing, nanofluidic ionic memristors have been rapidly developed for mimicking the ionic mechanisms of biological neurons and synapses. In these systems, designs and syntheses of nanosized pores, channels and 2D-slits are required to accomplish the memristive mechanisms. This study proposes another mechanism to develop an ionic memristor, which is based on a closed electrochemical bipolar cell with a designed bipolar electrode (BPE). Under an applied potential, the different electrochemical reactions on both sides of the BPE would lead to a memristive response with diode-like rectification. More importantly, a bipolar electrochemical memristor allows easy tuning of the response by simply varying the range of the applied electric potential. With a simple and scalable fabrication based on electrodeposition, the present system has great potential for use in neuromorphic architectures.

## 1. Introduction

Neuromorphic computing, an emulation of the brain's neural network and synapses, is being rapidly researched as a more energy-efficient and faster computational method.[1] Memristors are ideally suited as the basis for neuromorphic computing hardware and architecture,[2,3] given their ability to retain memory by switching or changing their resistance based on the history of the charge flowing through them.[4] To date, various electrical,[5] optoelectronic,[6] and ionic memristors have been reported.[7] Electrical memristors typically rely on the movement of ions (like oxygen vacancies) or the formation and rupture of conductive filaments within a thin film material. They are highly compatible with existing silicon-based manufacturing processes and can achieve high density and scalability.[8] However, the scaling of electrical connections can limit their

School of Metallurgy and Materials, University of Birmingham, Edgbaston, Birmingham, B15 2TT, UK. E-mail: k.w.kwan@bham.ac.uk

performance and density, and repeated electrical read/write cycles can cause unwanted changes to the stored resistance state.[9] Optoelectronic memristors leverage both electrical signals and light to change their resistance. They show the potential for high-speed, low-crosstalk, and energy-efficient parallel processing, but achieving robust all-optical control is difficult.[10]

To mimic ionic-based biological neurons, energy-efficient nanofluidic ionic memristors that realize data processing and storage by ion transports have been developed.[7,11,12] Although ionic memristors, at present, show a slower switching speed compared to other types of memristors due to the slower physical movement of ions, the research has been rapid because of the potential to emulate ion-mediated biological neural networks. The present mechanisms are mainly based on the ion transport across designed nanoscale pores,[13,14] channels,[15,16] and 2D-slits,[17,18] from an electrolyte reservoir to another under an applied voltage. The mechanisms employed, such as double layer polarization, ionic Coulomb blockage, ion adsorption/desorption, and concentration polarization,[7,11,12] are achieved through the design and synthesis of nanostructures that generally require sophisticated technology. A device with less demanding fabrication would be beneficial, and developing new memristive mechanisms at this early stage of ionic neuromorphic computing is also advantageous to the research field for offering more potential candidates for neuromorphic architectures.

In this study, we exploit bipolar electrochemistry for developing an ionic memristor. With a closed bipolar electrochemical cell making use of a solid electrode instead of pores or channels to separate two reservoirs, currents will be conducted by electron flow inside the electrode under an applied potential. Opposite poles are induced on the electrode and hence the name bipolar electrode (BPE).[19] The cell's current–voltage (I–V) characteristics are found to be dependent on the electrochemical reactions of the BPE, and we have achieved diode-like memristive characteristics of hysteresis and rectification resembling previous devices based on ion transport across the reservoirs.[15,17,20–23] The I–V characteristics of our bipolar electrochemical memristor can be

controlled by several methods, such as varying the potential window or applying a constant potential across or onto the BPE, thus creating a tuneable device that is highly desirable.[3] Furthermore, the main fabrication step of the BPE involves only electrodeposition, a process that is fast, simple and scalable, as elaborated by previous studies.[24,25] These features of I–V tuneability and ease of fabrication are highly beneficial to the development of neuromorphic computing.

## 2. Results

### 2.1. Design and mechanism of the bipolar electrochemical memristor

The BPE of the closed bipolar electrochemical cell is designed to be asymmetric with gold (Au) on one side and manganese dioxide ($MnO_2$) on the other, which can undergo different electrochemical reactions at the two electrode/electrolyte interfaces. The Au and $MnO_2$ layers are supported by a porous polymeric film as shown in Fig. 1a, which is selected to be a polycarbonate track-etch (PCTE) membrane with straight pores of diameter 10–15 nm.[26] With PCTE, the Au side of the BPE has a much smaller contact area with the electrolyte than the $MnO_2$ side, and the electrochemical reaction rate—an extensive quantity—will become slower.[27] The scanning electron microscopy (SEM) image of the structure shows a thin Au layer of thickness $\sim 100$ nm and a solid $MnO_2$ layer of thickness $\sim 2.5$ $\mu$m (Fig. 1b). The Au surface at the interface with $MnO_2$ is rough,

and nanopillars resulting from deposition into the pores of the PCTE are found on the other side. Materials characterization by energy-dispersive X-ray spectroscopy (EDX) and X-ray diffraction (XRD) confirms the compositions of the electrodeposited Au and $MnO_2$ (Fig. 1c and d), and the XRD shows that the $MnO_2$ obtained is poorly crystallized δ-birnessite.[28]

The electrolyte selected is sodium sulphate ($Na_2SO_4$), which is compatible with $MnO_2$ in performing electrochemical redox reactions.[29] Two interfaces of $MnO_2/Na_2SO_4$ and $Au/Na_2SO_4$ are formed on the BPE (Fig. 2a). A rectifying I–V behaviour is obtained via cyclic voltammetry (CV), and a pinched hysteresis loop with a cross-point potential ($V_{cp}$) of about 0.2 V is found (Fig. 2b).

The current of the cell is sustained by the electrochemical reactions of $MnO_2/Na_2SO_4$ and $Au/Na_2SO_4$—presumably the oxidation/reduction of $MnO_2$,[19] that of Au accompanied by oxidation adsorption/desorption of $SO_4^{2-}$ onto/from the Au surface,[30,31] and possibly the oxygen evolution reaction (OER) on Au. The applied potential is split among the two interfaces, in a way that the one with a lower limiting current gets a larger portion.[32] Unlike a conventional 3-electrode setup for measuring one solid/electrolyte interface where the potential difference across the interface is controlled, a closed bipolar electrochemical cell has two polarized interfaces in series between two electrodes, as illustrated in Fig. S1, SI. Under an applied potential difference $E$, the same current passes through the in-series interfaces, and in the present case, this current should be sustained by a redox reaction on the $MnO_2/Na_2SO_4$ interface: $MnO_2 + Na^+ + e^- \leftrightarrow MnOONa$,[29] and different possible reactions
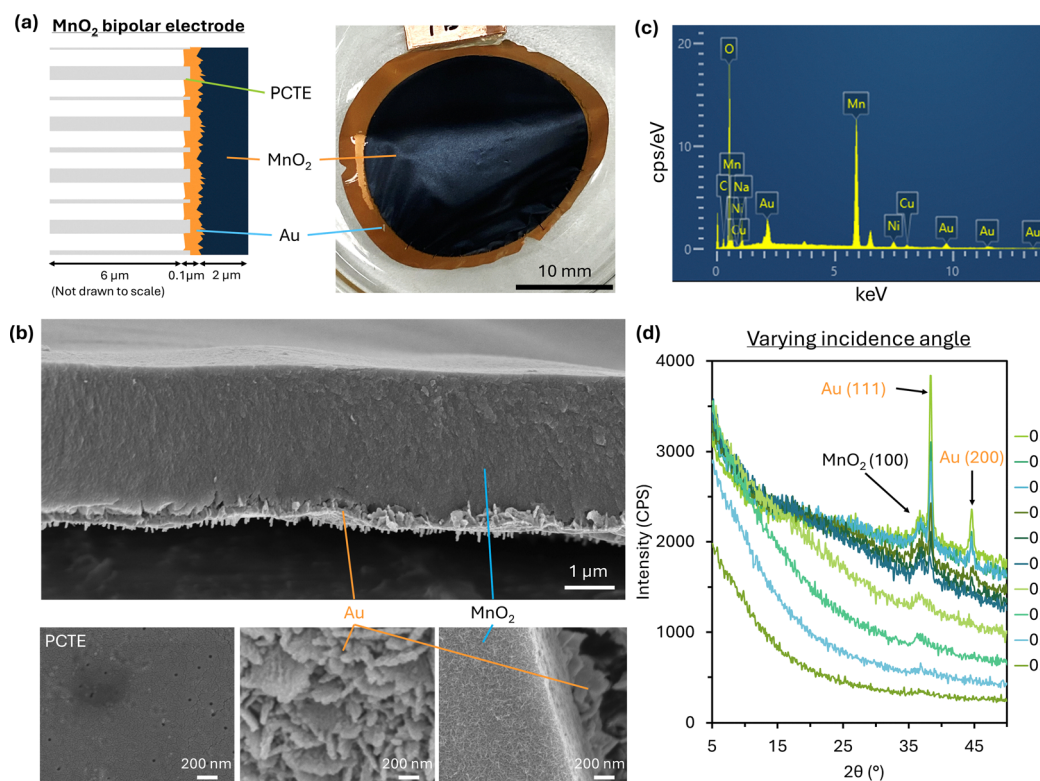


**Fig. 1** (a) Schematic and a photograph of the $MnO_2$ BPE and (b) SEM images of the cross-section of the $MnO_2$ BPE with the PCTE removed and the top views of PCTE, Au and $MnO_2$. (c) EDX and (d) XRD patterns of the $MnO_2$ BPE.
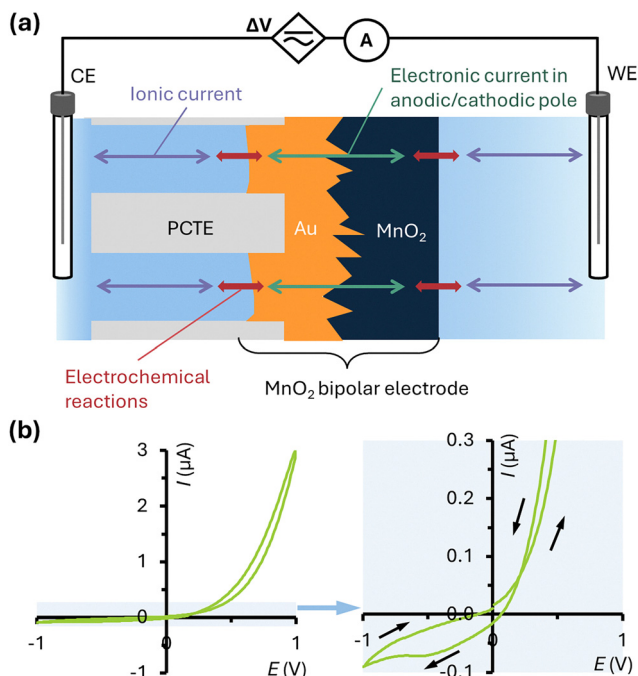
**(a)**



**(b)**



Fig. 2  (a) Schematic of the bipolar electrochemical memristor and (b) the corresponding I–V curves under CV. PCTE pore diameter: 15 nm, 0.5 mM Na$_2$SO$_4$, scan rate: 0.01 V s$^{-1}$.

on the Au/Na$_2$SO$_4$ interface: redox of Au that can follow different reaction paths,[33,34] adsorption/desorption of SO$_4^{2-}$ on the Au surface and even oxygen evolution (OER) on Au.[31] However, the potential difference across each of the interfaces ($E_a$, $E_c$) is generally unknown *a priori*, because the limiting currents of the two interfaces may be different.[32] The limiting currents depend on the electrochemical reactions, the areas of the interfaces, the bulk concentration and diffusivity of the reactant species, and the mass transport conditions on both sides. The interface with a smaller limiting current is identified as the limiting pole and the other is the excess (or coupling) pole. For the present BPE, Au/Na$_2$SO$_4$ is the limiting pole because of the smaller interfacial area due to the nano-porous PCTE. A larger portion of the applied potential difference would be partitioned to the limiting pole, as it requires a larger driving force to maintain the current. Therefore, the ratio between the limiting current of the poles ($\varepsilon$) is the chief parameter that defines the features of the CV response.[32] By choosing suitable interfaces, the current may reflect the combined electrochemical reactions on both poles, achieving the desired I–V responses.

As shown in Fig. 2b, no current peaks are observed under positive potential when the MnO$_2$ BPE is employed (15-nm PCTE, 0.5 mM Na$_2$SO$_4$, 0.01 V s$^{-1}$). This is because the redox reactions of MnO$_2$/Na$_2$SO$_4$ generally do not show any current peaks,[29,35] and the anodic peak of the Au/Na$_2$SO$_4$ interface should be small. The large current should be sustained by the redox of MnO$_2$/Na$_2$SO$_4$ and the oxidation, adsorption and OER occurring on the Au/Na$_2$SO$_4$ interface. Under negative potential, a small current peak responsible for the desorption

of Au/Na$_2$SO$_4$ is found at $\sim -0.5$ V, but apart from this, no other peaks are observed and the current remains small under negative potential because of the stable I–V behaviour of MnO$_2$/Na$_2$SO$_4$ over a larger potential window and the absence of the OER on the MnO$_2$/Na$_2$SO$_4$ interface.[29] The nature of the hysteresis can be deduced from the I–V curves at various scan rates. At slower scan rates (0.04 V s$^{-1}$ for 0.5 mM Na$_2$SO$_4$ and 1 V s$^{-1}$ for 5 mM), the hysteresis is insignificant, and a fast enough scan rate is required to result in hysteresis. A possible reason is that the electrochemical reaction of MnO$_2$ is sluggish due to the low concentration of Na$_2$SO$_4$, which could cause the current to increase further in the backward scan after the reversal at +1 V until the cross-point potential ($V_{cp}$) is reached. The sluggish reaction can also explain why the current decreases with the scan rate after the initial rise. A large potential drop from the high solution resistance can also lead to a decrease.[36] The non-zero $V_{cp}$ observed is likely caused by the influence of surface charges,[37] which arise on the BPE as the oxidation states of MnO$_2$ and Au are not completely reversed by applying the same magnitude of potential differences in the opposite polarity.

To further study the mechanism, several control experiments were performed. In the first one, we fabricated a MnO$_2$ BPE with a 30-nm PCTE, which would give a higher interfacial area on the Au side. Under CV, the I–V curve shows a completely different shape from that of 15-nm or 10-nm PCTE, with little rectification and neither hysteresis nor pinched loop (Fig. 3a). Significant current peaks at 0.53 V and $-0.39$ V are found, which correspond to the redox or adsorption/desorption of the Au/Na$_2$SO$_4$ interface. This indicates that the larger pores of PCTE allow a larger reaction rate on the interface. Compared to 15-nm PCTE (Fig. 2b), the difference in the position of the negative peak could be a result of the decrease in $\varepsilon$ as the interfacial area increases. A lower $\varepsilon$ would cause an anodic shift of the I–V and widening of the peak-to-peak separation—the potential difference between the anodic and cathodic peak.[32]

In the second control experiment, the electrolyte was changed from Na$_2$SO$_4$ to NaCl or KCl. The I–V curves of NaCl and KCl have smaller rectification where the positive currents are lower and the negative ones are higher (Fig. 3b). The hysteresis, however, is larger than that of Na$_2$SO$_4$. As NaCl and KCl have the same anion and a similar I–V, the difference from Na$_2$SO$_4$ should be caused by the anion Cl$^-$. As the size of Cl$^-$ is smaller than that of SO$_4^{2-}$, the diffusion in the pores of PCTE is easier, which results in the higher negative currents. Although the reaction rate of the Au/NaCl or Au/KCl interface is faster than that of Au/Na$_2$SO$_4$, the change in $\varepsilon$ is uncertain because the reactions at the MnO$_2$ interface are also faster with Cl$^-$ ions.[35] Therefore, the positive current is lower and the I–V hysteresis is larger even though the reaction rate at the Au interface increases. Nevertheless, from this experiment, we can see that the electrolyte plays an important role in the I–V feature of the closed bipolar electrochemical cell with the MnO$_2$ BPE. Further tests on the BPE without MnO$_2$ were conducted, which confirmed that the rectifying and hysteretic I–V of the former is achieved by the MnO$_2$/Na$_2$SO$_4$ interface, as discussed in the SI.
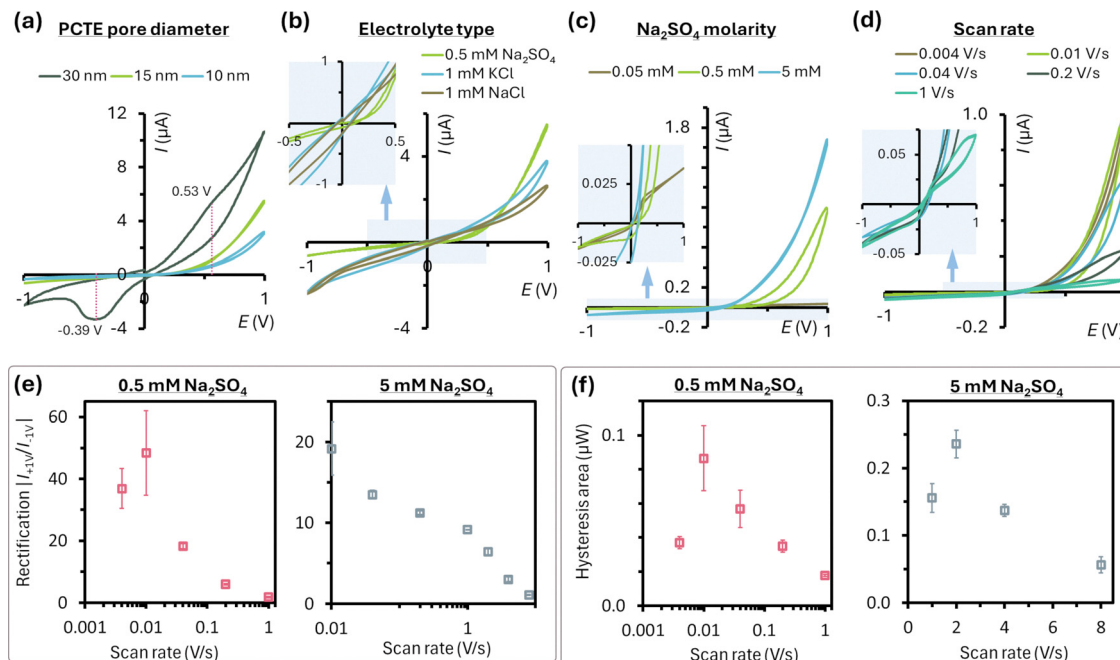
**Fig. 3** $I-V$ plots of the bipolar electrochemical memristor: (a) with different pore diameters of PCTE (0.5 mM $Na_2SO_4$, 0.01 V $s^{-1}$); (b) with different electrolytes: 0.5 mM $Na_2SO_4$, 1 mM KCl and 1 mM NaCl (15-nm PCTE, 0.01 V $s^{-1}$); (c) with different $Na_2SO_4$ concentrations (0.01 V $s^{-1}$, 15-nm PCTE); and (d) at different scan rates (0.5 mM $Na_2SO_4$, 10-nm PCTE). Plots of (e) rectification ($|I_{+1V}/I_{-1V}|$) and (f) area of the hysteresis loop against the scan rate for 0.5 mM and 5 mM $Na_2SO_4$ (10-nm PCTE).

## 2.2. Performance and control of the memristor

Tests with varying $Na_2SO_4$ concentrations reveals little rectification effect at a low molarity of 0.05 mM. Although a small hysteresis can still be observed, the shape of the $I–V$ curve is antisymmetric as shown in Fig. 3c, which is significantly different from the rectifying behaviour achieved by higher concentrations. Increasing the scan rate decreases the current for 0.05 mM, as shown in Fig. S2, SI, and at 0.2 V $s^{-1}$, the current oscillates significantly due to the limited current sensitivity of the electrochemical workstation. For 0.5 mM $Na_2SO_4$, good rectification and hysteresis are observed until the scan rate reaches 0.2 V $s^{-1}$, as shown in Fig. 3d, and the $I–V$ characteristics at 1 V $s^{-1}$ resemble the antisymmetric behaviour in 0.05 mM $Na_2SO_4$. Similarly, for 5 mM $Na_2SO_4$, good rectification and hysteresis can be observed until 2 V $s^{-1}$ (Fig. S3, SI), and higher scan rates again give an antisymmetric $I–V$ behaviour similar to 0.05 mM $Na_2SO_4$. Moreover, hysteresis disappears at lower scan rates from 0.01 to 0.2 V $s^{-1}$, similar to 0.5 mM $Na_2SO_4$ at 4 mV $s^{-1}$. For both 0.5 and 5 mM $Na_2SO_4$, the rectification ratio decreases with the scan rate in general, except for slightly smaller rectification at the lowest scan rate (4 mV $s^{-1}$) for 0.5 mM $Na_2SO_4$ (Fig. 3e). The highest rectification ratio recorded is $\sim 50$, which is comparable to previous ionic diodes.[38,39] The area of the hysteresis loop shows an initial rise, followed by a general decrease for both concentrations, as shown in Fig. 3f. From these results, we deduce that, at a given concentration, the scan rate has to be sufficiently fast for hysteresis to occur. A slower scan rate would allow the electrochemical reactions to take place reversibly, thereby suppressing hysteresis. Conversely, an excessively fast

scan rate does not allow sufficient time for the reactions to occur, resulting in an antisymmetric $I–V$ curve. Therefore, the scan rate should be selected within an optimal range for a given concentration to achieve the best rectifying and hysteretic $I–V$ curve. The cross-point potential ($V_{cp}$) of 0.5 mM $Na_2SO_4$ first increases and then decreases gradually, and that of 5 mM $Na_2SO_4$ only decreases, as shown in Fig. S4, SI. Also, comparing the $I–V$ at the same scan rate of 1 V $s^{-1}$, the lower concentration gives a lower $V_{cp}$. These results indicate that the $I–V$ mechanism is different from previous ion transport memristors.[15,20]

In addition to CV, chronoamperometry under step potentials from +1 V to −1 V was performed to show the fast switching speed of the rectification. The current–time ($I–t$) curves show the transient responses with a typical time constant of $\sim 0.1$ s, as seen from the spikes in Fig. 4a at the time for potential switching. The cathodic currents reach steady states in about 0.1 s, and their magnitudes keep decreasing during the step. In contrast, the anodic currents keep increasing under +1 V and take about 5 s to reach steady states. For step potential durations ($T_E$) longer than $\sim 30$ s, a significant rise of the current is usually observed in the first +1 V steps applied from 0 V but not subsequently—this indicates that the current depends on the history of applied potential. The rectification, calculated as the ratio of the current magnitude at +1 V just before stepping down to −1 V and that at −1 V just before stepping back to +1 V at the end of the $T_E$,[39] first increases considerably from $T_E = 10$ s to 20 s and then decreases steadily as $T_E$ increases to 60 s (Fig. 4b). The highest rectification ratio obtained is 12–13 with $T_E = 20 – 30$ s, which is smaller than that
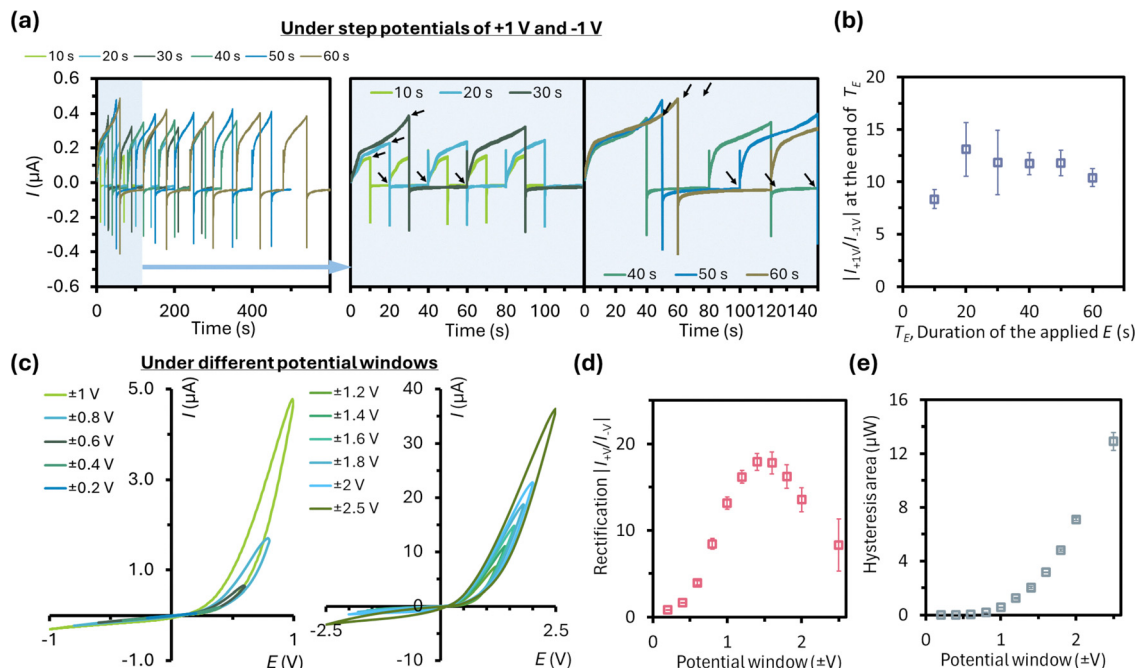
Fig. 4 (a) $I$–$t$ plots of the bipolar electrochemical memristor under chronoamperometry step potentials of +1 V and −1 V with step durations ($T_E$) of 10 s to 60 s and the magnified plots. Black arrows indicate the data taken for calculating $|I_{+1V}/I_{-1V}|$. (b) Plot of $|I_{+1V}/I_{-1V}|$ against $T_E$ (0.5 mM $Na_2SO_4$, 10-nm PCTE). (c) $I$–$V$ plots under potential windows of ±0.2 V to ±1 V and ±1.2 V to ±2.5 V and (d) the corresponding $|I_{+1V}/I_{-1V}|$ and (e) area of the hysteresis loop against the potential window (0.5 mM $Na_2SO_4$, 0.04 V s$^{-1}$, 10-nm PCTE).

obtained under CV with a triangular potential waveform that has a slightly longer duration for anodic and cathodic scans, e.g. ~18 at a scan rate of 0.04 V s$^{-1}$. These two observations imply that the magnitude and duration of the applied potential significantly affect the current response, such that a higher anodic current may lead to a higher cathodic one, and vice versa. To test this, we attempted widening the potential window to +1.2 V, which indeed gives a larger cathodic loop as shown in Fig. S5a, SI. Conversely, widening the window to −1.2 V only slightly increases the anodic peak (Fig. S5b, SI).

If the potential window is varied by the same amount at both ends, a set of similar $I$–$V$ curves will be obtained, as shown in Fig. 4c. For ±0.2 V, the rectification and hysteresis are almost absent (Fig. S6, SI). Then, a wider window gives a higher rectification until ±1.4 V (Fig. 4d). After that, the cathodic current is increased significantly to result in a lower rectification. The area of the hysteresis loop, however, increases exponentially with the potential window (Fig. 4e). At ±2.5 V, the data scatter is larger than the others, presumably because electrochemical reactions such as the OER or the hydrogen evolution reaction (HER) have occurred quickly on the BPE at such large potentials to produce unstable current.[40] Nonetheless, the above results show that $I$–$V$ is dependent on the history of the potential applied, and the rectification and hysteresis can be tuned by varying the potential window.

Based on the results of chronoamperometry and CV with varying potential windows, we found another way to tune the $I$–$V$ by first applying a constant potential from one reservoir to the other for some time and then measured the $I$–$V$ by CV. As shown in Fig. 5a, applying +1 V for 5 min increases the subsequent CV anodic and cathodic current significantly and shrinks the hysteresis of the anodic side while enlarging the cathodic one. The changes can be reversed by applying −1 V for the same duration. If the constant potential applied is increased to +1.5 V, the current will increase further, and the hysteresis for the cathodic current will also be enlarged more. Again, the changes can be reversed by −1.5 V. The $I$–$t$ plots corresponding to the ±1 V and ±1.5 V potential steps show that positive potentials lead to much higher currents that continuously increase over the entire duration, whereas negative potentials make the currents decrease in magnitude over time (Fig. S7, SI). The increasing currents under positive potential steps suggest that the rate of electrochemical reactions of the BPE—cathodic for $MnO_2/Na_2SO_4$ and anodic for $Au/Na_2SO_4$—both increase steadily, which may involve the reduction of $MnO_2$ to $MnOONa$, oxidation of Au, adsorption of $SO_4^{2-}$ onto Au and the OER on Au. Therefore, after the positive potential step, as the subsequent CV scans positively from 0 V, the sustained positive potential leads to the higher current observed. Moreover, the potential step causes the positive current to become steady, and therefore the subsequent CV will have a smaller hysteresis. The cathodic current also increases when the scan enters the cathodic side, because the cell has just undergone an extended period of anodic potential application (from both the step and the anodic side of the CV). This mirrors the effect observed when increasing the potential window. The hysteresis is also larger because the cathodic current has a more rapid rate.

A similar way for tuning the $I$–$V$ is demonstrated by applying constant potentials directly onto the BPE, as shown in Fig. 5b. This approach also allows the current to be reversibly increased and decreased. The Au layer allows potentials to be applied directly
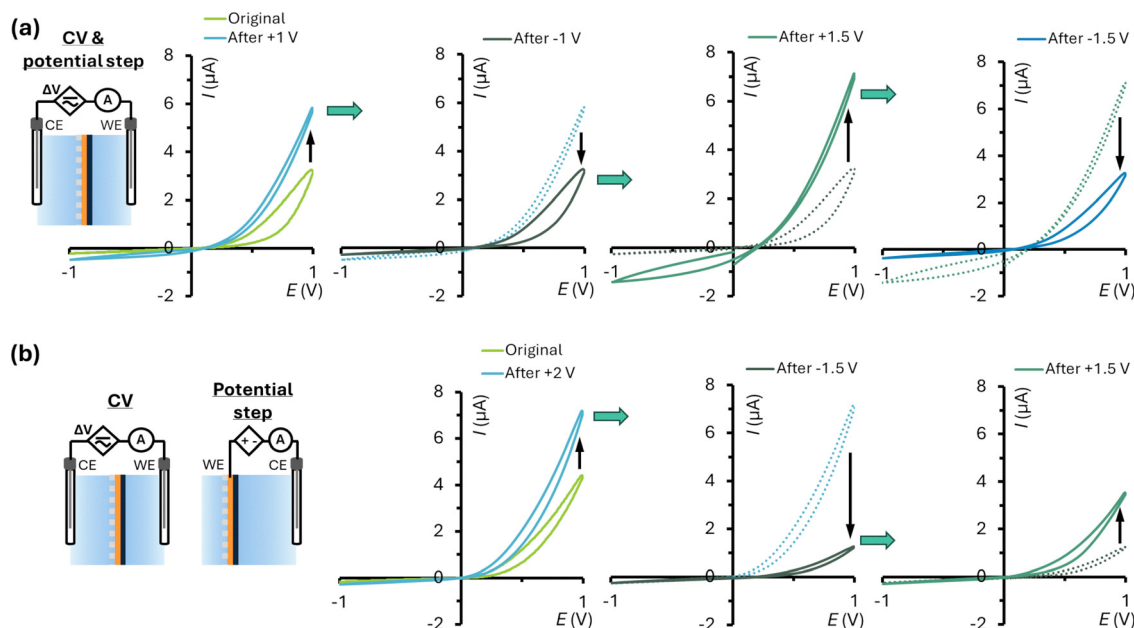
Fig. 5 Tuning the $I-V$ curves of the bipolar electrochemical memristor by applying constant potential (a) across the bipolar electrode (BPE) with +1 V, −1 V, +1.5 V and −1.5 V for 5 min and (b) directly onto the BPE with +2 V, −1.5 V and +1.5 V for 5 min (0.5 mM $Na_2SO_4$, 0.04 V $s^{-1}$ for CV, 10-nm PCTE).

onto the BPE. Similar to the previous method, a positive potential applied onto the BPE will increase the anodic current significantly and a negative one will reverse the effect (Fig. 5b). However, as the positive potential step is now directly applied to the BPE against the right reservoir, the $MnO_2/Na_2SO_4$ would be oxidized, in contrast to the situation in the previous method where $MnO_2/Na_2SO_4$ is reduced by the positive potential across the BPE. The $I-t$ plots of the potential steps show that the negative potential applied onto the BPE gives a higher current magnitude than the positive one (Fig. S8, SI), suggesting that the reduction rate of $MnO_2/Na_2SO_4$ is higher than its oxidation rate. Therefore, after applying a positive potential directly to the BPE, the anodic current under CV increases because the oxidized $MnO_2/Na_2SO_4$ has become more readily reduced. In contrast, the cathodic side of the $I-V$ curve exhibits no significant change. This is because only the $MnO_2/Na_2SO_4$ has been oxidized in this direct potential application method, unlike the previous method where both $Au/Na_2SO_4$ and $MnO_2/Na_2SO_4$ were altered by the potential step across the BPE. In summary, the $I-V$ of the closed bipolar electrochemical cell can be altered by applying potentials across the BPE which induces electrochemical reactions on both interfaces or to the BPE that induces the reactions on $MnO_2$. Finally, the endurance under multiple CV cycles was checked, and a good stability over 30 cycles is observed (Fig. S9, SI). Future work on endurance and retention at the high-resistance state (HRS) and the low-resistance state (LRS) is required to further validate the performance of the memristor.

## 3. Conclusions

In summary, a tuneable ionic diode-like memristor has been developed using a closed bipolar electrochemical cell with a $MnO_2$ BPE. The mechanism is based on the different electrochemical reactions on both sides of the BPE achieved by the asymmetric electrode/electrolyte interfaces. The $I-V$ characteristics, including the rectification ratio and the area of the hysteresis loop, can be tuned by varying the potential windows of the CV and by applying constant potentials across or directly onto the BPE, showing that the mechanism can become a valuable option for developing ionic memristors in neuromorphic computing.

## Conflicts of interest

The authors declare no competing financial interest.

## Data availability

The data supporting this article have been included as part of the SI. Experimental methods, supplementary figures, and supplementary notes on the diode-like memristive mechanism (PDF). See DOI: **https://doi.org/10.1039/d5tc02764k**

## Acknowledgements

## References

1 A. Noy and S. B. Darling, *Science*, 2023, **379**, 143–144.
2 A. Thomas, *J. Phys. D: Appl. Phys.*, 2013, **46**, 093001.
3 D. Marković, A. Mizrahi, D. Querlioz and J. Grollier, *Nat. Rev. Phys.*, 2020, **2**, 499–510.
4 D. B. Strukov, G. S. Snider, D. R. Stewart and R. S. Williams, *Nature*, 2008, **453**, 80–83.

5 S. H. Jo, T. Chang, I. Ebong, B. B. Bhadviya, P. Mazumder and W. Lu, *Nano Lett.*, 2010, **10**, 1297–1301.

6 L. Hu, J. Yang, J. Wang, P. Cheng, L. O. Chua and F. Zhuge, *Adv. Funct. Mater.*, 2021, **31**, 2005582.

7 G. Xu, M. Zhang, T. Mei, W. Liu, L. Wang and K. Xiao, *ACS Nano*, 2024, **18**, 19423–19442.

8 M.-K. Song, J.-H. Kang, X. Zhang, W. Ji, A. Ascoli, I. Messaris, A. S. Demirkol, B. Dong, S. Aggarwal and W. Wan, *ACS Nano*, 2023, **17**, 11994–12039.

9 J. Domaradzki, D. Wojcieszak, T. Kotwica and E. Mańkowska, *Int. J. Electron. Telecommun.*, 2020, 373–381.

10 S. Shrivastava, H. Juliano, P. A. L. Uong and T.-Y. Tseng, *APL Electron. Devices*, 2025, **1**, 021506.

11 Y. Hou, Y. Ling, Y. Wang, M. Wang, Y. Chen, X. Li and X. Hou, *J. Phys. Chem. Lett.*, 2023, **14**, 2891–2900.

12 B. Xie, T. Xiong, W. Li, T. Gao, J. Zong, Y. Liu and P. Yu, *Chem. – Asian J.*, 2022, **17**, e202200682.

13 J. Feng, K. Liu, M. Graf, D. Dumcenco, A. Kis, M. Di Ventra and A. Radenovic, *Nat. Mater.*, 2016, **15**, 850–855.

14 G. Paulo, K. Sun, G. Di Muccio, A. Gubbiotti, B. Morozzo della Rocca, J. Geng, G. Maglia, M. Chinappi and A. Giacomello, *Nat. Commun.*, 2023, **14**, 8390.

15 T. Xiong, C. Li, X. He, B. Xie, J. Zong, Y. Jiang, W. Ma, F. Wu, J. Fei and P. Yu, *Science*, 2023, **379**, 156–161.

16 T. Emmerich, Y. Teng, N. Ronceray, E. Lopriore, R. Chiesa, A. Chernev, V. Artemov, M. Di Ventra, A. Kis and A. Radenovic, *Nat. Electron.*, 2024, **7**, 271–278.

17 P. Robin, T. Emmerich, A. Ismail, A. Niguès, Y. You, G.-H. Nam, A. Keerthi, A. Siria, A. Geim and B. Radha, *Science*, 2023, **379**, 161–167.

18 P. Robin, N. Kavokine and L. Bocquet, *Science*, 2021, **373**, 687–691.

19 A. Gamero-Quijano, A. F. Molina-Osorio, P. Peljo and M. D. Scanlon, *Phys. Chem. Chem. Phys.*, 2019, **21**, 9627–9640.

20 D. Wang, M. Kvetny, J. Liu, W. Brown, Y. Li and G. Wang, *J. Am. Chem. Soc.*, 2012, **134**, 3651–3654.

21 Q. Sheng, Y. Xie, J. Li, X. Wang and J. Xue, *Chem. Commun.*, 2017, **53**, 6125–6127.

22 X. Zhou, Y. Zong, Y. Wang, M. Sun, D. Shi, W. Wang, G. Du and Y. Xie, *Natl. Sci. Rev.*, 2024, **11**, nwad216.

23 P. Ramirez, V. Gómez, J. Cervera, S. Mafe and J. Bisquert, *J. Phys. Chem. Lett.*, 2023, **14**, 10930–10934.

24 C. Zhang, Y. Li, H. Li, Q. Zhang and J. Lu, *J. Mater. Chem. C*, 2021, **9**, 374–394.

25 C. Zhang, Y. Li, Z. Li, Y. Jiang, J. Zhang, R. Zhao, J. Zou, Y. Wang, K. Wang and C. Ma, *ACS Appl. Mater. Interfaces*, 2022, **14**, 3111–3120.

26 P. Apel, *Radiat. Meas.*, 2001, **34**, 559–566.

27 S. Trasatti and O. Petrii, *J. Electroanal. Chem.*, 1992, **327**, 353–376.

28 Y. Munaiah, B. G. S. Raj, T. P. Kumar and P. Ragupathy, *J. Mater. Chem. A*, 2013, **1**, 4300–4306.

29 S. C. Pang, M. A. Anderson and T. W. Chapman, *J. Electrochem. Soc.*, 2000, **147**, 444.

30 M. B. Cortie, A. Maaroof and G. Smith, *Gold Bull.*, 2005, **38**, 14–22.

31 Z. Shi, J. Lipkowski, M. Gamboa, P. Zelenay and A. Wieckowski, *J. Electroanal. Chem.*, 1994, **366**, 317–326.

32 E. Laborda, J. López-Asanza and A. Molina, *Anal. Chem.*, 2023, **95**, 17311–17317.

33 S. Brummer and A. Makrides, *J. Electrochem. Soc.*, 1964, **111**, 1122.

34 K. Ogura, S. Haruyama and K. Nagasaki, *J. Electrochem. Soc.*, 1971, **118**, 531.

35 R. N. Reddy and R. G. Reddy, *J. Power Sources*, 2004, **132**, 315–320.

36 A. J. Bard, L. R. Faulkner and H. S. White, *Electrochemical methods: fundamentals and applications*, John Wiley & Sons, 2022.

37 D. Wang, W. Brown, Y. Li, M. Kvetny, J. Liu and G. Wang, *ChemElectroChem*, 2018, **5**, 3089–3095.

38 D. He, E. Madrid, B. D. Aaronson, L. Fan, J. Doughty, K. Mathwig, A. M. Bond, N. B. McKeown and F. Marken, *ACS Appl. Mater. Interfaces*, 2017, **9**, 11272–11278.

39 B. R. Putra, K. J. Aoki, J. Chen and F. Marken, *Langmuir*, 2019, **35**, 2055–2065.

40 Y. Zhao, C. Chang, F. Teng, Y. Zhao, G. Chen, R. Shi, G. I. Waterhouse, W. Huang and T. Zhang, *Adv. Energy Mater.*, 2017, **7**, 1700005.